

Hybrid Organic Semiconductors Including Chalcogen Atoms in π -Conjugated Skeletons. Tuning of Optical, Redox, and Vibrational Properties by Heavy Atom Conjugation

Juan Casado, María Moreno Oliva, Mari C. Ruiz Delgado, Rocío Ponce Ortiz, J. Joaquín Quirante, and Juan T. López Navarrete*

Department of Physical Chemistry, University of Málaga, Campus de Teatinos s/n, Málaga 29071, Spain

Kazuo Takimiya and Tetsuo Otsubo

Graduate School of Engineering, Hiroshima University, 1-4-1 Kagamiyama, Higashi-Hiroshima, 739-8527, Japan

Received: February 23, 2006; In Final Form: April 18, 2006

In this work, the interactions between heteroatoms (S, Se, and Te) and conjugated skeletons are analyzed. The study is carried out by using electronic absorption and fluorescence spectroscopies, electrochemistry, vibrational Raman spectroscopy, and theoretical calculations in the framework of DFT and TD-DFT theories. Optical spectra are described in terms of one-electron promotions between orbitals around the energy gap. Electrochemistry, in the framework of the Koopman's approach, is also interpreted. The vibrational Raman spectra are assigned to molecular modes and the evolution changing the heteroatom is addressed and an effective tuning of these properties is found. Part of this modulation is associated with local electronic interactions depending on the relative S, Se, and Te electronegativities. Unconventional long-range heteroatom–heteroatom interactions have been proposed which arise from the existence of effective π -conjugated channels. The molecular level understanding of structure–property relationships in these organic/inorganic semiconductors are of great interest in the interdisciplinary area of material science.

I. Introduction

Alternative semiconducting materials for thin-film field-effect transistors (TFTs), which might show electron mobilities at least comparable to that of amorphous silicon and with extra-engineering advantages (i.e., mechanical flexibility, capability of covering large substrate areas, processing at low-temperature deposition conditions with low-cost methods, etc.) are required to enable new opportunities for display and storage technologies.^{1–4} Small conjugated molecules (i.e., short chain oligomers) have received great attention as new semiconductor substrates for TFTs. Among these organics phenylene oligomers², oligothiophenes derivatives,³ and fused aromatic compounds (i.e., pentacene)⁴ have shown the most promising performances.

Any progress in the design of new conjugated systems should be conducted by well-established structure–property relationships. These guidelines must consider molecular-scale electronic properties (i.e., redox potentials, HOMO–LUMO energies, optical and redox band gaps, molecular structure and conformation, chemical stability, etc.) as well as supramolecular parameters (i.e., electron/hole mobility, crystal structure, thin film microstructure, threshold voltages, etc.). As for the first case, π -conjugated skeletons have been modified with proper organic functions deriving in a great deal of device improvements.^{1–4} Much less attention, however, has been devoted to the combination of heavy inorganic atoms with organic π -conjugated cores. For instance, in the case of oligothiophenes, their oligosele-nophene homologues have been studied only in a few reports, and none is found to be referring to the heavier parents.⁵

Takimiya et al. have exploited a very interesting synthetic approach to easily incorporate chalcogen atoms into π -carbonated backbones or 2,6-diphenylbenzo[1,2-*b*:4,5-*b'*] dichalcogenophenes⁶ (Figure 1). From a fundamental perspective, this chalcogen family of compounds brings the opportunity of studying the electronic coupling of aromatic thiophene, selenophene and tellurophene with benzene in extended conjugated systems pursuing improved electronic features. From a practical point of view, these hybrid dichalcogenophenes have been tested as semiconductors in TFTs and proved to exhibit tunable p-channel conductivities, a fact that has an important repercussion in the field of organic electronics.⁶

For the last years, our research interest has been focused on the analysis of the electronic properties of π -conjugated systems, trying to elucidate how fundamental interactions between atoms in molecules determine emerging properties of interest in material science. An example of this strategy is the influence of the phenomenon of electron delocalization in some of the operational characteristics of organic TFT devices based in conjugated molecules. Very appealing for us is the detection of great changes in the Raman spectra of the above-mentioned dichalcogenophenes by a simple change of the heteroatom (vide infra). It must be mentioned that Raman spectroscopy is well suited to deal with conjugated molecules,⁷ so that very important items such as π -electron delocalization extent or conjugation length, nature of charge defects, intramolecular charge transfer processes, etc., have been successfully addressed by its consideration. The reliability of this technique relies in the existence of an effective *electron–phonon* mechanism which explains, among other findings, the simplicity of the Raman spectra of conjugated molecules. An enormous Raman activity is detected

* To whom correspondence should be addressed. (J.C) casado@uma.es; (J. T. L. N.) teodomiro@uma.es.



Figure 1. Chemical structures and nomenclatures for the compounds studied in this work.

for those vibrational modes involved in the relevant conjugated paths (i.e., C=C/C–C stretching modes) owing to the significant polarization of the electronic clouds within their atomic motions. Therefore, our starting hypothesis is that *the changes in the Raman spectra* of these three molecules are a consequence of the affectation of their conjugational properties by the electronic nature of the heavy atom. Nonetheless, the heteroatom dependence of the molecular properties is not restricted to the Raman response, and a rather subtle dependence of their optical and electrochemical properties is also observed. This series of experimental findings deserves a more detailed inspection, which motivates the understanding of the lying property–structure relationships.

This work analyzes a set of spectroscopic (i.e., electronic absorption and emission and Raman) and electrochemical properties of the above presented 2,6-diphenylbenzo[1,2-*b*:4,5-*b'*] dichalcogenophenes. The modulation of the π -conjugational properties by the insertion in the same organic π -conjugated skeleton of heteroatoms (i.e., group VI) will be analyzed. The whole experimental study is supported with quantum chemical calculations in the framework of density functional theory.

II. Experimental and Computational Details

The synthesis of these 2,6-diphenylbenzo[1,2-*b*:4,5-*b'*] dichalcogenophenes (Figure 1) has been already reported.⁶ Electrochemical data were obtained in benzonitrile (i.e., PhCN) at 150 °C recording their cyclic voltammeteries at a scan rate of 100 mV/s, with two Pt wires as the working and counter electrodes and Ag/AgCl electrode as the reference. Tetrabutylammonium hexafluorophosphate (i.e., (TBA)PF₆) at a 0.1 M concentration was used as supporting electrolyte. All the data were calibrated against Fc/Fc⁺.

Absorption and emission spectra are obtained in CH₂Cl₂ or THF. UV–vis–NIR absorption spectra were recorded either on a Lambda 19 Perkin-Elmer dispersive spectrophotometer or an Agilent 8453 instrument equipped with a diode array detection system. Emission spectra were measured using a JASCO FP-750 spectrofluorometer. No fluorescent contaminants were detected upon excitation in the wavelength region of experimental interest. Solutions were prepared with an absorbance between 0.1 and 0.2 at the wavelength region of experimental interest. FT-Raman spectra were measured using an FT-Raman accessory kit (FRA/106-S) of a Bruker Equinox 55 FT-IR interferometer. A continuous-wave Nd:YAG laser working at 1064 nm was employed for excitation. A germanium detector operating at liquid nitrogen temperature was used. Raman scattering radiation was collected in a backscattering configuration with a standard spectral resolution of 4 cm^{−1}. To avoid possible damage to the oxidized samples upon laser radiation its power was kept at a level lower 20 mW and 1000–3000 scans were averaged for each spectrum.

Density functional theory methods have become very popular since the inclusion of electron correlation effects with accuracies comparable to those of correlated ab initio procedures, such as MP2, while very much reducing the computational costs of the latter.⁸ Hence, the use of low-cost computational DFT procedures has demonstrated very satisfactory to analyze conjugated molecules where electron correlation plays a decisive role. Furthermore, harmonic force fields obtained by DFT have

proved to be more effective than those based in traditional Hartree–Fock (HF) approaches.⁹ Therefore, ground-state total energies, equilibrium geometries, eigenfrequencies, and normal coordinates for our conjugated chalcogen samples were calculated by using density functional theory. Calculations were carried out by means of the Gaussian-03 package of programs.¹⁰ The Becke's three parameter (B3) gradient-corrected exchange functional combined with the correlation Lee–Yang–Parr (LYP) functional is used.¹¹ As recommended for DFT calculations and taking into account the presence of heavy atoms, the polarized double- ζ split valence (DZVP) orbital basis set is chosen.¹² Details of the modelization are as follows: (i) Optimal geometries were determined on isolated entities and neither solvent nor counteranions effects were considered. (ii) All the geometrical parameters were left to vary independently during the optimization. (iii) On the resulting ground-state optimized geometries, harmonic vibrational frequencies and Raman intensities were calculated numerically. (iv) Ab initio calculations can be expected to yield vibrational frequencies with an accuracy of about 10% compared to the respective experimental values. Only to improve the numerical comparison, calculated harmonic vibrational frequencies are uniformly scaled down by a random factor (0.97) to best fit the experimental quantities.⁹ All quoted theoretical vibrational frequencies reported are thus scaled values.

The time-dependent DFT (TD–DFT) approach is now being widely applied in both chemistry and condensed matter physics to describe electron excitations.¹³ While not as accurate for excitations as the ordinary DFT is for ground state properties, this theory has a considerable predictive power and is computationally quite tractable. Excited-states calculations, considering vertical electronic excitation energies, and oscillator strengths were computed by using the TD–DFT approach. At least the 30 lowest-energy electronic excited states were computed for all the molecules. TD–DFT calculations were done using the same functional (B3LYP) and basis set (DZVP).

III. Molecular and Electronic Structures

The three molecules are predicted to be nearly planar with averaged deviations of 3–5° for the outermost phenyls relative to the central fused part. At the level of the core, the interaction of the VI group heteroatoms with our organic skeleton might be described by the consideration of the following effects: (i) C/X electrostatic forces due to their different electronegativities. (ii) The possible extension of the chalcogen atom valence shell accompanied by a change in its hybridization. (iii) Formation of a delocalized π -system, stabilized by conjugation, and further favored by the rigidity of the chalcogen–chalcogen path. The visualisation of these effects is sketched in Scheme 1 through the description of hypothetical resonant forms.

Figure 2 displays the B3LYP/DZVP optimized geometries and relevant Mülliken atomic charges, and Scheme 1 displays the relevant resonant or canonical forms whose interplay or superposition describes most of the molecular features predicted by B3LYP/DZVP calculations: (i) Resonant forms **A** and **B** represent the largest conjugated paths, where heteroatom intervention is excluded. (ii) Resonant form **C** couples electronically the two heteroatoms through the largest “external” CC

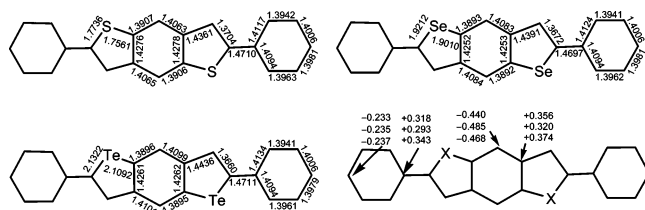
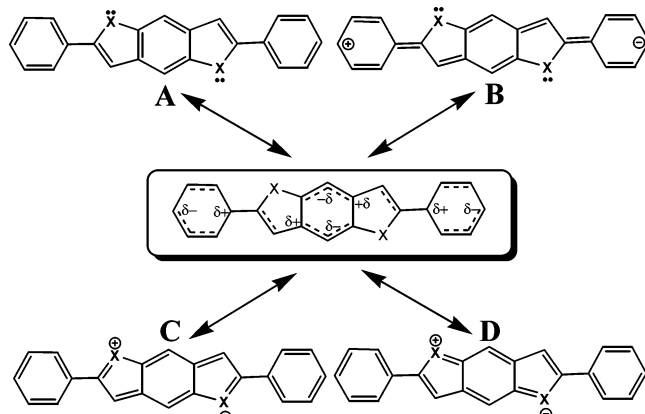


Figure 2. DFT/B3LYP/DZVP optimized geometries (in Å) and relevant Mulliken atomic charges for the chalcogen samples. Charge values read from the top to the bottom for S, Se, and Te, respectively.

SCHEME 1: Resonant Forms and Schematic Representation of the Optimized Geometry of DPh-BDS in Terms of Single and Double Bonds.



conjugated path. (iii) Resonant form **D**, finally, accounts for the interaction of these heavy atoms via a shorter or “internal” CC path.

The central structure in Scheme 1 represents the optimized geometries of these molecules, where dotted bonds account for distances in the ≈ 1.37 – 1.41 Å interval, having the remaining bonds longer lengths. In this simple representation of the calculated structure, contributions of each resonant form are noticed. For example, let us consider the following points.

(i) Though to quite different extents, the structure of the central ring is contributed by the four resonant forms.

(ii) The structures of the five members ring are mainly determined by resonant forms **A** and **D** (i.e., stressing the absence of aromatic character for these rings).

(iii) The great impact of resonant form **D** might justify the asymmetry between the bond lengths of the innermost (i.e., shorter)/outermost (i.e., larger) C–X bonds.

(iv) Conjugation of the outermost phenyl rings toward the central fused core is described by resonant form **B**. However, the large bond distance of the CC bond connecting these phenyls with the core highlights its low contribution.

(v) The overlapping of these “competitive” conjugating channels occurs at the level of the central six-member ring originating its seemingly dearomatization. Regarding this hypothesis, the BLA parameter (i.e., bond length alternation degree defined as the mean average between the consecutives CC bond lengths of a given path) can be used to evaluate bond length equalization that is near to zero for benzenoid rings, while the opposite can be interpreted as aromaticity’s rupture (i.e., typical BLAs of 0.100 Å are characteristic of full quinoid rings).¹⁴ The BLAs of the central rings deviate from zero in the three samples (i.e., 0.0235 Å in DPh-BDS, 0.0240 Å in DPh-BDSe, and 0.0244 Å in DPh-BDTe). This theoretical picture stresses the partial aromaticity breaking of the central ring (i.e., minor role of the proaromatic resonant form **A**) and the greater impact of

the other conjugative paths, two of them promoted by the heteroatoms.

For DPh-BDS, the bond length equalization of the internal path described by resonant form **D** is remarkable (BLA = 0.018 Å), what contrasts with those of resonant forms **C** (0.037 Å) and **B** (0.039 Å). The low BLA predicted for the resonant form **D** might agree with the existence of a bonding/nonbonding interaction in the HOMO orbital between the heteroatom and the neighbor C atoms of this CC path (vide infra, Figure 3). On the other hand, the relatively large BLA of resonant form **B** (i.e., including the CC bonds connecting the core and the outermost rings) would imply a certain rotational degree of freedom (i.e., accentuated in solution by conformational distortions as detected in the optical spectra).

Regarding B3LYP/DZVP calculated charges, it is quite remarkable that the largest amounts of negative charge correspond to those carbon atoms of the central six-member ring in which the four resonant forms overlap in between. These atoms (see Scheme 1, Figure 3) always have nonzero atomic coefficients in the wave functions of the occupied orbitals. On the contrary, positive charges on this central ring are concentrated in atoms with negligible contributions to the HOMO orbital wherein the resonant forms cross over or bifurcate.

Let now further inspect the topologies of the frontier molecular orbitals in Figure 3 to get more insights of the electronic structure from the perspective of the postulated resonant forms. For the HOMO orbital of the three compounds, the interaction of the heavy atom and the two vicinal carbon atoms is more favored for the inner one resulting from the antibonding/nonbonding coupling of the external/internal C–X bonds. Furthermore, an increasing contribution of the heteroatom is seemingly noticed for the heavier ones (i.e., larger values of their atomic coefficients in the HOMO). This would mean that more polarizable electrons (i.e., $S < Se < Te$) enter into play for the internal CC path thus facilitating π -electron delocalization on it. Another interesting feature is the bonding interaction between the heteroatom and the outer neighbor C in the HOMO-1 orbital of DPh-BDS that might cause its strengthening in agreement with the prediction of resonant form **C** (i.e., this resonant form converts the C–S bond in a C=S one). As for the LUMO orbitals, bonding interactions between those atoms connected with double bonds in the resonant form **B** are found. The sign of the coupling between the atoms describing the resonant form **A** is not detected in the orbitals around the gap, what might be in agreement with the absence of benzenoid character of the central six-member ring (i.e., resonant form **A** predicts this feature).

IV. Optical Spectra

Figure 4 shows the absorption and emission spectra of the three compounds, and Figure 5 displays the DFT/B3LYP/DZVP energy level diagram for the frontier orbitals around the gap together with the TD-DFT/B3LYP/DZVP transition energies and corresponding oscillator strengths.

Regarding the groups of bands around 350 and 380 – 420 nm, the following characteristics are observed:

(i) The bands at higher energy are always stronger.

(ii) TD-DFT/B3LYP/DZVP calculations predict the greatest oscillator strengths (i.e., except for DPh-BDS) to be accumulated into the theoretical lines at 350 nm in agreement with the observation of the strongest bands of the UV-vis spectra at these wavelengths.

(iii) The longest wavelength bands show a progressive red-shifting in the series. However, a different displacement is

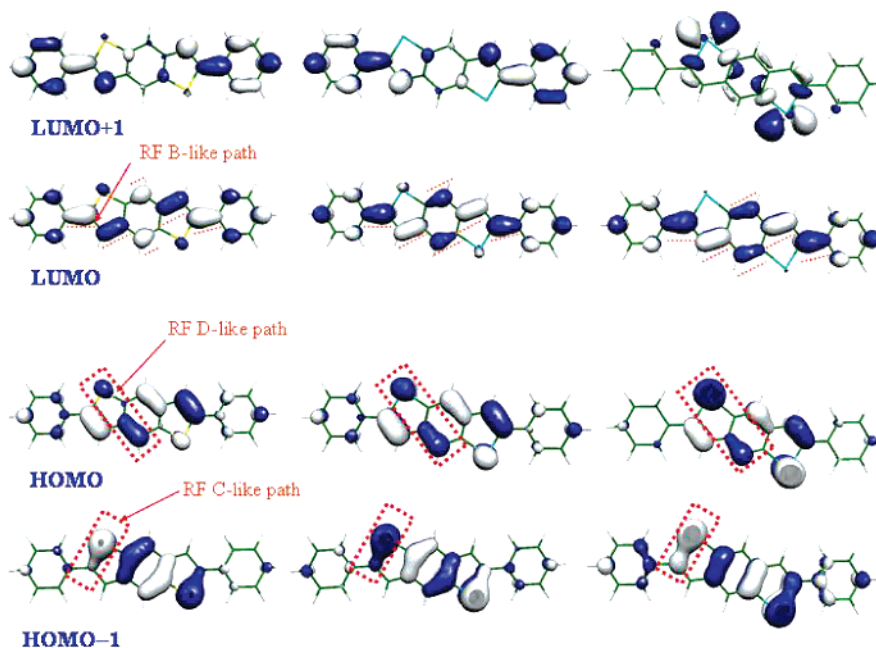


Figure 3. DFT/B3LYP/DZVP molecular orbital topologies for the most relevant terms of each compound (RF, resonant form in Scheme 1; left, DPh-BDS; middle, DPh-BDSe; right, DPh-BDTe).

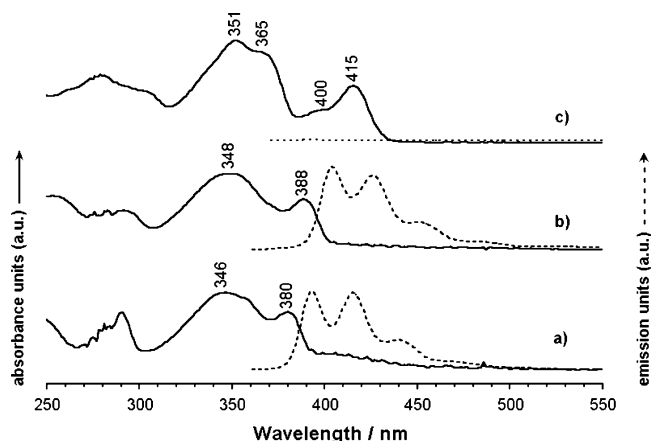


Figure 4. Absorption (solid line) and fluorescence spectra (dotted line) of the three compounds in THF and CH_2Cl_2 respectively: (a) DPh-BDS; (b) DPh-BDSe; (c) DPh-BDTe.

noticed on DPh-BDS \rightarrow DPh-BDSe (8 nm) than in DPh-BDSe \rightarrow DPh-BDTe (27 nm). Theory accurately reproduces the whole red-shifting (i.e., 39 nm in theory, 35 nm in experiment) on passing from DPh-BDS to DPh-BDTe and the concomitant displacement in the series, 390 (theory) and 380 (experiments) nm in DPh-BDS, 401 and 388 nm in DPh-BDSe, and 429 and 415 nm in DPh-BDTe.

(iv) In detriment of this good comparison, the bands around 350 nm, which scarcely move in the UV-vis spectra, are predicted to red-shift up to by 31 nm.

TD-DFT/B3LYP/DZVP calculations allow us to describe the configurations of these electronic excitations in terms of one-electron promotions between occupied and unoccupied orbitals around the gap. For DPh-BDS, the first excited state is calculated at 390 nm (experimentally at 380 nm) with oscillator strength (f) of 0.92. This band corresponds with the $S_0 \rightarrow S_1$ excitation and is mainly (85%) composed by the HOMO \rightarrow LUMO one-electron transition, with a minor contribution (negative sign for its dipole transition moment, $[\mu_{if}]$) from the one-electron HOMO-1 \rightarrow LUMO transition. The $S_0 \rightarrow S_2$ theoretical feature is predicted at 351 nm (experimen-

tally at 346 nm) with $f = 0.49$ in DPh-BDS and is described by a superposition of the following one-electron transitions: HOMO-1 \rightarrow LUMO (72% and positive $[\mu_{if}]$), HOMO \rightarrow LUMO+2 (17%, and negative $[\mu_{if}]$) and HOMO \rightarrow LUMO (12% and positive $[\mu_{if}]$). Table 1 summarizes the one-electron transition contributions to the first excited states of the three derivatives. The most noticeable observation is the increasing mixing of configurations for the first excitations in the molecules with heavier atoms likely due to correlation effects when more polarizable electrons enter into play. An example of this mixing is the change in the orbital description of the $S_0 \rightarrow S_2$ (i.e., 366 nm/H-1 \rightarrow L in DPh-BDSe and 388 nm/H \rightarrow L + 1 in DPh-BDTe) and of the $S_0 \rightarrow S_3$ (i.e., 324 nm/H \rightarrow L + 1 in DPh-BDSe and 382 nm/H-1 \rightarrow L in DPh-BDTe) excitations.

There occurs a destabilization/stabilization of the HOMO/LUMO terms by 0.0770/0.1108 eV on going from DPh-BDS to DPh-BDTe, which might account for the red-shifting of the lowest energy band in the UV-vis spectra. The decreasing efficiency (i.e., atomic orbital overlapping) in the bonding interaction described in section III for the HOMO between the heteroatom orbital and the neighbor carbon (i.e., internal path) for the three molecules might be the reason for the predicted destabilization. Though the participation of the heavy atoms in the LUMO is less significant than in the occupied terms, there is still some contribution (see Figure 3) which decreases in the series, being negligible in DPh-BDTe. Bearing in mind that this interaction is of antibonding nature, a stabilization of this LUMO orbital in the series might be expected. This HOMO/LUMO destabilization/stabilization is commonly found in conjugated molecules upon conjugation increment. Moreover, this finding might result from the electronic interaction within the internal path as a consequence of inorganic atom involvement. In this regard, section V (i.e., vibrational Raman study) will outline some structural and spectroscopic results supporting this hypothesis.

In the emission spectra the following characteristics are noticed:

(i) DPh-BDTe shows no fluorescence emission likely due to the effective singlet \rightarrow triplet intersystem crossing channels favored by spin-orbit couplings mediated by d and f high

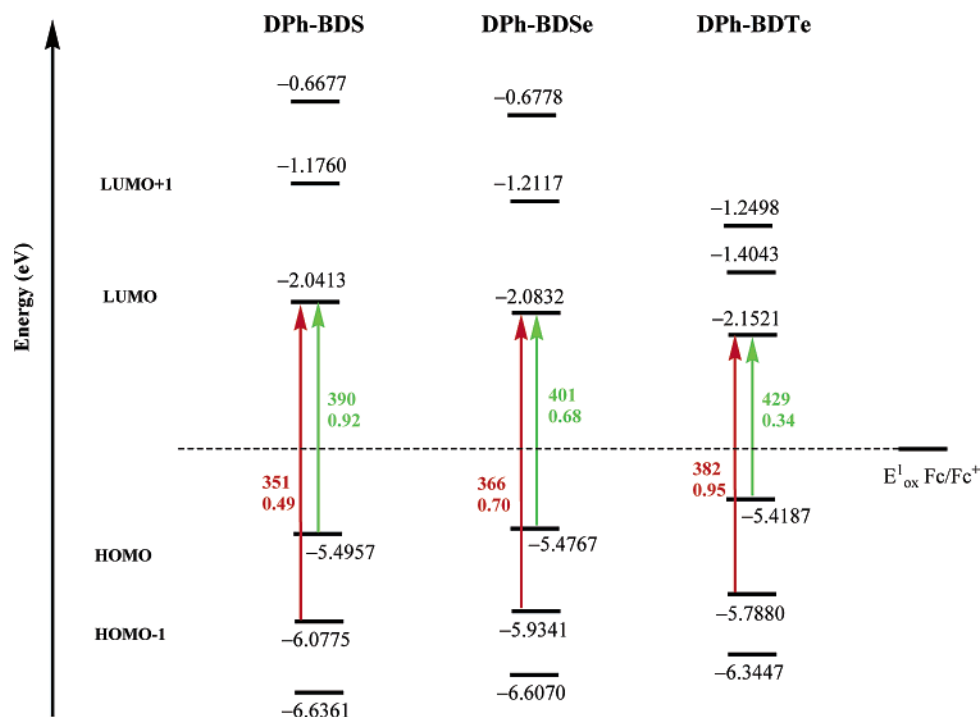


Figure 5. DFT/B3LYP/DZVP energy diagram for the orbitals around the gap. Energy transitions and oscillator strengths for the more important one-electron promotions are shown.

TABLE 1: TD-DFT/B3LYP/DZVP Data for the First Three Excited Lowing Lying Energy States^a

	$S_0 \rightarrow S_1$	$S_0 \rightarrow S_2$	$S_0 \rightarrow S_3$
DPh-BDS	390 nm, $f = 0.92$ H \rightarrow L (+0.638) H-1 \rightarrow L (-0.116)	351 nm, $f = 0.49$ H-1 \rightarrow L (+0.651) H \rightarrow L + 2 (-0.152) H \rightarrow L (+0.102)	319 nm, $f = 0.00$ H \rightarrow L + 1 (+0.628) H-2 \rightarrow L (-0.302)
DPh-BDSe	401 nm, $f = 0.68$ H \rightarrow L (+0.627) H-1 \rightarrow L (+0.184)	366 nm, $f = 0.70$ H-1 \rightarrow L (+0.641) H \rightarrow L (-0.162) H \rightarrow L + 2 (+0.116)	324 nm, $f = 0.00$ H \rightarrow L + 1 (+0.629) H-2 \rightarrow L (+0.301)
DPh-BDTe	429 nm, $f = 0.34$ H \rightarrow L (+0.629) H-1 \rightarrow L (-0.212) H-1 \rightarrow L + 4 (+0.104)	388 nm, $f = 0.00$ H \rightarrow L + 1 (+0.672) H-2 \rightarrow L + 3 (-0.143) H-1 \rightarrow L + 1 (-0.105)	382 nm, $f = 0.95$ H-1 \rightarrow L (+0.629) H \rightarrow L (+0.180)

^a H and L denote the highest energy occupied molecular orbital and lowest energy unoccupied molecular orbital.

energy atomic orbitals of tellurium. Taking into consideration that the $S_0 \rightarrow S_1$ excitation receives some contribution from the LUMO+4 term (Table 1), the absence of emission is supported by the involvement of Rydberg states of Te in these higher energy states. Apparently, these states do not participate in the description of S_1 in the other two compounds and fluorescence quenching is less appreciable.

It is observed a significant asymmetry between absorption and fluorescence spectra of DPh-BDS and DPh-BDSe that should be ascribed to torsional mobility in the ground electronic state (S_0) as compared with the emissive state (S_1). This effect is due to the rotation around the single CC inter-ring bond and is typical of π -conjugated hydrocarbons with low energetic torsional modes around C-C single bonds such as α,α' -oligothiophenes¹⁵ or p,p' -oligophenylenes.¹⁶

The vibronic substructures of the fluorescence spectra (i.e., up to four bands spaced by 1450–1300 cm^{-1} are observed in the fluorescence spectra owing to vibronic progressions of the same $S_1 \rightarrow S_0$ deexcitation) are quite similar for the two samples indicating that the molecular structures of the emissive states are rather similar. In this regard, the Stokes's shifts steadily increases in the same way as the absorption maxima increase. This finding can be addressed by the minor contribution of the

heteroatoms to the LUMO (i.e., S_1 state) compared with the carbonated paths (i.e., identical in both compounds).

V. Electrochemical Data

Figure 6 displays the cyclic voltammetry waves of the three samples in PhCN 0.1 M (TBA)PF₆. Two irreversible processes in the anodic range are observed. Let assume the validity of the Koopman's approach¹⁷ (i.e., it relates the ionization potential (IP) with the potential of the reversible oxidation) in the following discussion. Furthermore, we are confident that the Koopman's approach still holds upon the restriction of its statements with two further constrains: (i) Oxidations are not reversible and (ii) IP energy is approached with the absolute HOMO energy considering that oxidation consists of the extraction of electrons from the highest occupied molecular orbital.

The first oxidation processes are shifted to less anodic potentials (i.e., 1.30 \rightarrow 1.26 \rightarrow 1.04 V on DPh-BDS \rightarrow DPh-BDSe \rightarrow DPh-BDTe). The absolute B3LYP/DZVP HOMO energies (i.e., Figure 5) show the same trend than oxidation potentials, thus a slight change on DPh-BDS \rightarrow DPh-BDSe and a greater downshifts on passing to the Te-derivative are

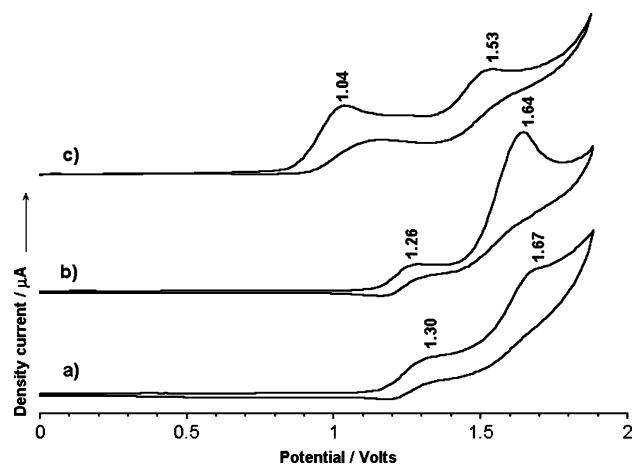


Figure 6. Cyclic voltammograms of (a) DPh-BDS, (b) DPh-BDSe, and (c) DPh-BDTe in PhCN 0.1 M (TBA)PF₆ at 150 °C. Scan rate of 100 mV/s, using as reference an Ag/AgCl electrode.

recorded. This comparison indicates that oxidation likely consists on one-electron extractions (i.e., difficult to deduce provided the irreversibility of the processes). If higher oxidation states were involved, then Koopman's approach would fail. Furthermore, this oxidation can be conceived as centered in the fused core because of the good correlation between heteroatom electronegativities (i.e., Pauling values, S = 2.58, Se = 2.55, and Te = 2.10) and peak potentials. This is in accordance with the role of heteroatoms as described by the resonant forms **C** and **D** (i.e., spreading only on the fused moiety). It must be mentioned that oxidations were obtained at 150 °C, hence the reasonably good quantitative experimental/theoretical correlation might indicate that the observed irreversibility would not be necessary associated with chemical degradation (i.e., for instance, unknown dependence of diffusion coefficient with T, etc.). This fact highlights the chemical stability of these substrates in p-channel semiconductors (i.e., air stability).

Second oxidation peak potentials are less sensitive to the inorganic atom and evolve by −0.14 V on passing from DPh-BDS to DPh-BDTe. Probably the generation of higher oxidation states (i.e., dications) might imply the increment of electrostatic repulsions what would separate injected charges far away from each other. If this effect really occurs the charged defects would be shared by the whole molecule and the portion of stabilizing effect coming from heteroatoms would decrease regarding the percentage in the case of the monocationic species.

This electrochemical analysis emphasizes the relevant participation of the heavy atoms in the description of the ground electronic properties through contributions to the HOMO and HOMO-1 wave functions. This heteroatom dependence of the electrochemical properties likely shares the same origin that the tuning of optical properties in section IV. To get further insights into the affectation of the molecular structures by conjugation of heavy atoms in organic skeletons, a careful interpretation of the vibrational Raman spectra closes the paper.

VI. FT-Raman Spectroscopic Data

This section pursues two main purposes. On one hand, the evolution of the vibrational Raman frequencies will be used as microscopic proofs of the changes in the molecular structures as a function of the heteroatom (Figure 7 shows these spectra). And on the other hand, the question raised in the Introduction about the changes on the Raman intensity within the three samples is attempted from the perspective of π -electron conjugation.

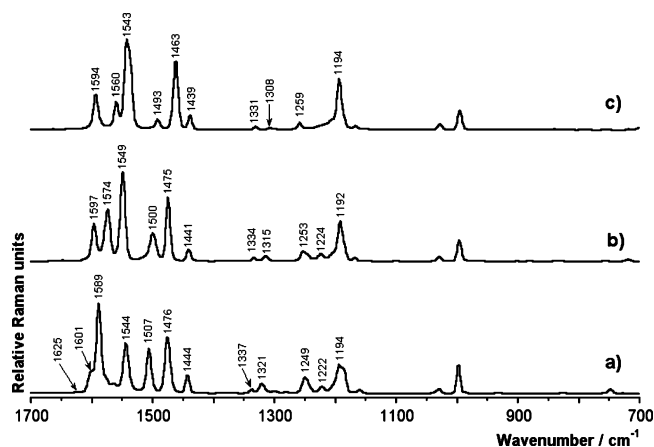


Figure 7. Solid-state FT-Raman spectra ($\lambda_{\text{exc}} = 1064$ nm) of (a) DPh-BDS, (b) DPh-BDSe, and (c) DPh-BDTe.

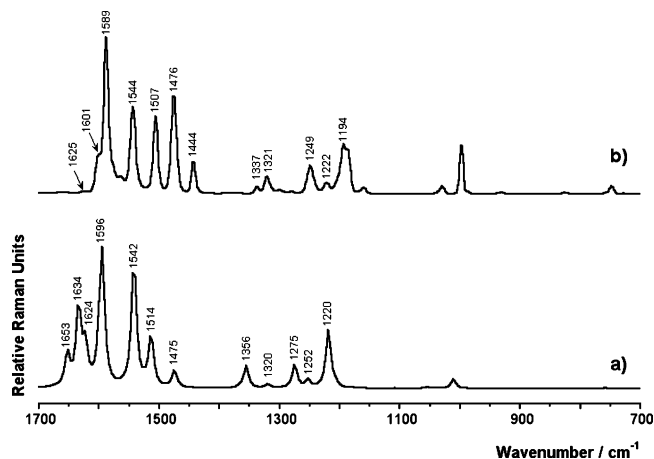


Figure 8. Comparison between the (a) DFT/B3LYP/DZVP Raman spectrum of DPh-BDS and (b) its solid-state FT-Raman spectrum ($\lambda_{\text{exc}} = 1064$ nm).

In both cases, an assignment of the main Raman bands is needed as the starting point of the interpretation. To this end, Figure 8 compares the DFT/B3LYP/DZVP (i.e., as an isolated entity in the vacuum) Raman spectrum of DPh-BDS with that in solid state, whereas Figure 9 depicts the calculated eigenvectors associated with the most important lines.

At a first glance, main changes in the spectra are noticed in the 1600–1450 cm^{−1} interval, which thus focuses our attention. Furthermore, and for these vibrations, displacements of the heavy atoms are not appreciable. A mass effect on the vibrational frequencies, consequently, should be discarded. In this spectral range, theory and experiment match satisfactorily what is sufficient for a general assignment of the experimental lines to internal coordinates.

(a) Assignment of DPh-BDS and Correlation. The medium-weak band at 1601 cm^{−1} (i.e., predicted at 1634 cm^{−1}) corresponds with a vibration of the central six-member ring located on the CC channel described by resonant form **D** (i.e., internal path). In this vibration, consecutive bonds stretch antisymmetrically with similar amplitudes. This line experiences a downshift upon substitution of sulfur by its two parents (i.e., 1574 cm^{−1} in DPh-BDSe and 1560 cm^{−1} in DPh-BDTe). This frequency behavior is typical of C=C/C–C stretching vibrations of conjugated systems when an increment of π -electron delocalization takes place. These findings are originated by the phenomenon of CC skeletal relaxation of the CC sequence where conjugation increment (i.e., bond length equalization) occurs. In this regard, the great downshift by 27 cm^{−1} on

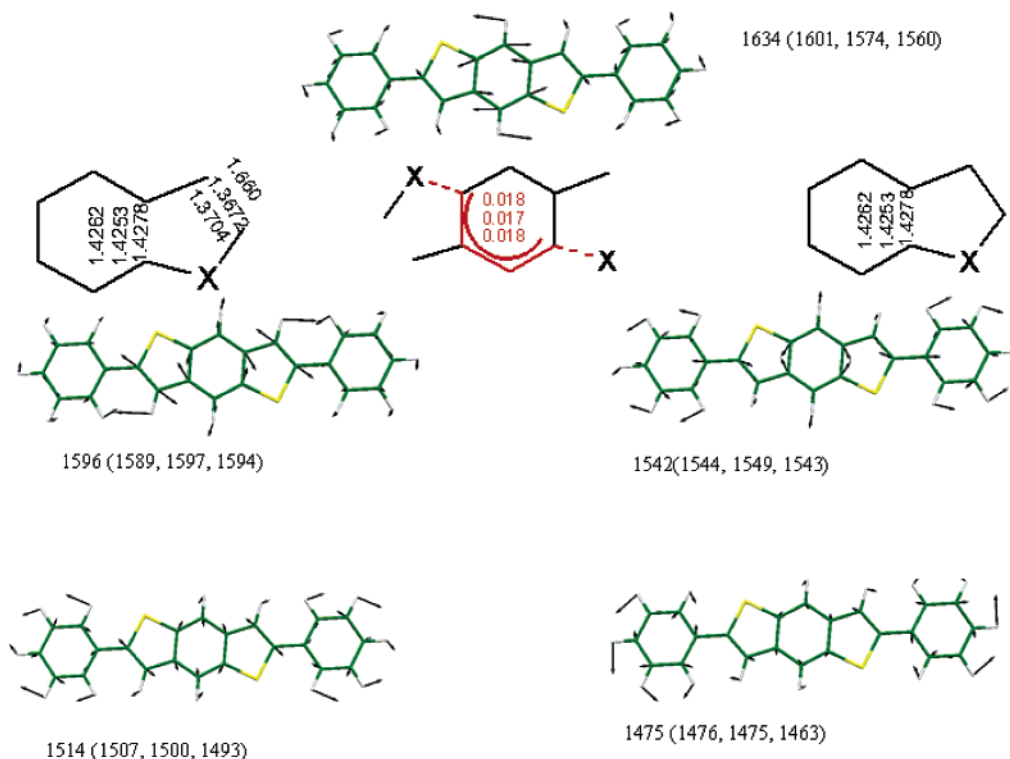


Figure 9. Vibrational eigenvectors associated with the most important lines of the DFT//B3LYP/DZVP theoretical Raman spectrum of DPh-BDS. The evolution of the distances for particular bonds are inserted in the figure. Frequency and bond lengths are given in cm^{-1} and Å respectively. In parentheses are given experimental values. In red is the BLA of the colored CC path.

changing sulfur by selenium might result from the active conjugation in this internal path what is supported by the decrease of the BLA from 0.018 Å in DPh-BDS to 0.017 Å in DPh-BDSe.

The following bands are due to vibrations of particular CC bonds instead of delocalized motions, thus a connection between their frequency evolution and that of the CC bond lengths (i.e., rather than collective features as the BLA) can be established. The most intense band of the spectrum at 1589 cm^{-1} (i.e., predicted at 1596 cm^{-1}) is assigned to an antisymmetric CC stretching of the five-members ring. This line evolves to 1597 cm^{-1} in DPh-BDSe and to 1594 cm^{-1} in DPh-BDTe. The wavenumber upshift can be accounted for the slight strengthening of the outer five-members ring CC bonds (i.e., 1.3704 Å in DPh-BDS, 1.3672 Å in DPh-BDSe, and 1.3660 Å in DPh-BDTe), while the $1597\text{ (DPh-BDSe)} \rightarrow 1594\text{ (DPh-BDTe)}$ cm^{-1} downward should be ascribed to the lengthening of its internal CC bond (i.e., 1.4252 Å in DPh-BDSe and 1.4261 Å in DPh-BDTe). The same atom motion of this bond in the five-members ring coupled with the CC stretch of the bond connecting the core to the external phenyl groups originates the scattering at 1544 cm^{-1} (i.e., predicted at 1542 cm^{-1}). This Raman feature correlates with those at 1549 cm^{-1} in DPh-BDSe and 1543 cm^{-1} in DPh-BDTe (i.e., the bond length change of this internal CC bond matches the evolution of the above frequencies: 1.4278 Å in DPh-BDS, 1.4253 Å in DPh-BDSe, and 1.4262 Å in DPh-BDTe).

In contrast to the above vibrations, the Raman lines at $1507/1476\text{ cm}^{-1}$ in DPh-BDS (i.e., predicted at $1514/1475\text{ cm}^{-1}$) move down to $1500/1475\text{ cm}^{-1}$ in DPh-BDSe and to $1493/1463\text{ cm}^{-1}$ in DPh-BDTe. These modes are due to CC stretch spreading, in a similar way, over the whole molecule (i.e., see Figure 9). The increment of π -electron delocalization in the central core upon heteroatom change can account for this

frequency downshift, though these vibrations cannot be ascribed to conjugational modes of one of the four paths described in section III.

(b) Raman Intensity and Electronic Structure. Let now attempt to understand the changes in the intensity pattern of the Raman spectra for the three samples (i.e., this observation called our attention in the Introduction). This finding can be summarized as the selective enhancement of the mode associated with the band at 1544 cm^{-1} in DPh-BDS (i.e., 1549 cm^{-1} in DPh-BDSe and 1543 cm^{-1} in DPh-BDTe) and the Raman activity depression within the series of the band at 1589 cm^{-1} DPh-BDS (i.e., 1597 cm^{-1} in DPh-BDSe and 1594 cm^{-1} in DPh-BDTe). The Raman activity of a given line is proportional to the changes in the molecular polarizability (α) during the associated vibrational motion. As a matter of fact, this polarizability term of the equation of Raman intensity is dominated by the dipolar moment transition (i.e., term of pure electronic contribution) changes when electronic excitation in the Raman experiment occurs in the contour of the strongest electronic absorption band.¹⁸ In these conditions, the largest contributions to Raman activity must come from the lowest lying energy electronic transition (i.e., the HOMO \rightarrow LUMO transition). Our main hypothesis in this work is the existence of an internal CC path connecting both heteroatoms in which π -electron delocalization or conjugation effectively takes place and increases for heavier inorganic atoms. If this phenomenon really takes place, this CC fragment must be the part of the molecule where polarization of the electronic cloud in the presence of an external electromagnetic field might occur more easily. The band that gets stronger in the series is located precisely in one bond of this internal path. The gaining contribution to the HOMO (i.e., see Figure 3) for heavier atoms might provide larger changes of the electronic polarizability within this path upon electromagnetic excitation thus explaining, qualitatively, the intensification of this band. On the other hand, the Raman line that

gets weaker in the series (i.e., that around 1590 cm⁻¹) spreads out this internal path and a loss of its intensity in the series is reasonably expected.

VII. Conclusions

In this work, the analysis of the interactions between heteroatoms and organic π -conjugated skeletons are addressed. A multidisciplinary analysis using optical and vibrational Raman spectroscopies, electrochemistry and theoretical model chemistry (i.e., DFT and TD-DFT theories) is carried out. 2,6-diphenylbenzo[1,2-*b*:4,5-*b'*] dichalcogenophenes (i.e., S, Se, and Te) are the compounds selected for this purpose. Additional interest of these samples arises from their use as semiconducting elements in p-channel FETs.

Absorption and fluorescence spectra have been carefully described in terms of one-electron promotions between orbitals around the energy gap. Electrochemistry has been understood in the framework of the Koopman's approach. Raman spectra have been ascribed to microscopic molecular vibrations, and correlation of vibrational frequencies and skeletal structures (i.e., property-structure relationships) for the three samples is proposed.

An effective tuning of the properties has been observed varying the heteroatom. To intuitively account for their role, a few of competing resonant forms have been proposed and their reliability tested by their impact in the experimental findings and theoretical results. A certain dependence of some properties with the electronegativity of the heavy atom is observed; however, interesting features are directly promoted by long-range interactions between the heavy atoms due to the existence of effective π -conjugated channels.

To the general reader of chemistry, this work contributes to shed light on the knowledge of the subtle electronic interactions occurring between inorganic atoms inserted in π -conjugated organic skeletons. The establishment of these types of structure-property relationships is of great importance in the interdisciplinary area of material science.

Acknowledgment. J.C. is grateful to the MEC of Spain for a Ramón y Cajal position of Chemistry at the University of Málaga. M.C.R.D. and R.P.O. are also indebted to the MEC and Junta de Andalucía, respectively, for personal grants. Research at the University of Málaga was supported by the Ministerio de Educación y Ciencia (MEC) of Spain through the project BQU2003-03194 and, and by the Junta de Andalucía (Grant FQM-0159) and through the "Modalidad B de Perfeccionamiento de Doctores en Centros fuera de Andalucía".

References and Notes

- (1) (a) Brown, A. R.; Pomp, A.; Hart, C. M.; de Leeuw, D. M. *Science* **1995**, *270*, 972. (b) Dimitrakopoulos, C. D.; Brown, A. R.; Pomp, A. *J. Appl. Phys.* **1996**, *80*, 2501. (c) Nelson, S. F.; Lin, Y. Y.; Gundlach, D. J.; Jackson, T. M. *Appl. Phys. Lett.* **1998**, *72*, 1854. (d) Herwig, P. T.; Mullen, K. *Adv. Mater.* **1999**, *11*, 480. (e) Rogers, J.; Bao, Z.; Baldwin, K.; Dodabalapur, A.; Crone, B.; Raju, V. R.; Katz, H. E.; Kuck, V.; Amundson, K.; Ewing, J.; Drziac, P. *Proc. Natl. Acad. Sci. U.S.A.* **2001**, *98*, 4835. (f) Sirringhaus, H.; Kawase, T.; Friend, R. H.; Shimoda, T.; Inbasekaran, M.; Wu, W.; Woo, E. P. *Science* **2000**, *290*, 2123. (g) Garnier, F. *Acc. Chem. Res.* **1999**, *32*, 209.
- (2) (a) Van Hutten, P. F.; Krasnikov, V. V.; Hadziioannou, G. *Acc. Chem. Res.* **1999**, *32*, 257. (b) Albolta, M.; Beljonne, D.; Bredas, J. L.; Ehrlich, J. E.; Fu, J. Y.; Heikal, A. A.; Hess, S. E.; Kogej, T.; Levin, M. D.; Mader, S. R.; Perry, J. W.; Rockel, H.; Rumi, M.; Subramaniam, G.; Webb, W. W.; Wu, X. L.; Xu, C. *Science* **1998**, *281*, 1653. (c) Hosokawa, C.; Higashi, H.; Kusumoto, T. *Appl. Phys. Lett.* **1993**, *62*, 3238. (d) Guha, S.; Graupner, W.; Resel, R.; Chandrasekhar, M.; Chandrasekhar, H. R.; Glaser, R.; Leising, G. *Phys. Rev. Lett.* **1999**, *82*, 3625. (e) Friend, R. H.; Gymer, R. W.; Holmes, A. B.; Burroughes, J. H.; Marks, R. N.; Taliani, C.; Bradley, D. D. C.; Dos Santos, D. A.; Brédas, J. L.; Lögdlund, M.; Salaneck, W. R. *Nature* **1999**, *397*, 121.
- (3) (a) Cornil, J.; Calbert, J.-P.; Beljonne, D.; Silbey, R.; Bredas, J.-L. *Adv. Mater.* **2000**, *12*, 978. (b) Facchetti, A.; Deng, Y.; Wang, A.; Koide, Y.; Sirringhaus, H.; Marks, T. J.; Friend, R. H. *Angew. Chem., Int. Ed.* **2000**, *39*, 4547. (c) Pappenfus, T. M.; Chesterfield, R. J.; Frisbie, C. D.; Mann, K. R.; Casado, J.; Raff, J. D.; Miller, L. L. *J. Am. Chem. Soc.* **2002**, *124*, 4184. (d) Facchetti, A.; Mushrush, M.; Katz, H. E.; Marks, T. J. *Adv. Mater.* **2003**, *15*, 33. (e) Facchetti, A.; Yoon, M.-H.; Stern, C. L.; Katz, H. E.; Marks, T. J. *Angew. Chem., Int. Ed.* **2003**, *42*, 3900. (f) Chesterfield, R. J.; Newman, C. R.; Pappenfus, T. M.; Ewbank, P. C.; Haukaas, M. H.; Mann, K. R.; Miller, L. L.; Frisbie, C. D. *Adv. Mater.* **2003**, *15*, 1278. (g) Newman, C. R.; Frisbie, C. D.; da Silva, D. A.; Brédas, J.-L.; Ewbank, P. C.; Mann, K. R. *Chem. Mater.* **2004**, *16*, 4436. (h) Yoon, M.-H.; DiBenedetto, S. A.; Facchetti, A.; Marks, T. J. *J. Am. Chem. Soc.* **2005**, *127*, 1348. (i) Takahashi, T.; Matsuoka, K.; Takimiya, K.; Otsubo, T.; Aso, Y. *J. Am. Chem. Soc.* **2005**, *127*, 8928.
- (4) (a) Dimitrakopoulos, C. D.; Brown, A. R.; Pomp, A. *J. Appl. Phys.* **1996**, *80*, 2501. (b) Siegrist, T.; Kloc, C.; Schön, J. H.; Batlogg, B.; Haddon, R. C.; Berg, S.; Thomas, G. A. *Angew. Chem., Int. Ed.* **2001**, *40*, 1732. (c) Gundlach, D. J.; Linn, Y. Y.; Jackson, T. N. *IEEE Electron Device Lett.* **1997**, *18*, 87. (d) Yoo, S.; Domercq, B.; Kippelen, B. *Appl. Phys. Lett.* **2004**, *85*, 5427. (e) Takimiya, K.; Kunugi, Y.; Toyoshima, Y.; Otsubo, T. *J. Am. Chem. Soc.* **2005**, *127*, 3605.
- (5) (a) Kunugi, Y.; Takimiya, K.; Toyoshima, Y.; Yamashita, K.; Aso, Y.; Otsubo, T. *J. Mater. Chem.* **2004**, *14*, 1367. (b) Kunugi, Y.; Takimiya, K.; Yamane, K.; Yamashita, K.; Aso, Y.; Otsubo, T. *Chem. Mater.* **2003**, *15*, 6. (c) Kunugi, Y.; Takimiya, K.; Yamashita, K.; Aso, Y.; Otsubo, T. *Chem. Lett.* **2002**, 958.
- (6) Takimiya, K.; Kunugi, Y.; Konda, Y.; Niihara, N.; Otsubo, T. *J. Am. Chem. Soc.* **2004**, *126*, 5074.
- (7) (a) Hernández, V.; Casado, J.; Ramírez, F. J.; Zotti, G.; Hotta, S.; López Navarrete, J. T. *J. Chem. Phys.* **1996**, *104*, 9271. (b) Casado, J.; Hernández, V.; Hotta, S.; López Navarrete, J. T. *J. Chem. Phys.* **1998**, *109*, 10419. (c) Casado, J.; Hernández, V.; Hotta, S.; López Navarrete, J. T. *Adv. Mater.* **1998**, *10*, 1258. (d) Casado, J.; Katz, H. E.; Hernández, V.; López Navarrete, J. T. *J. Phys. Chem. B* **2002**, *106*, 2488. (e) Zerbi, G. *Handbook of Conducting Polymers*; Marcel Dekker: New York, 1998. (f) Ruiz Delgado, M. C.; Hernández, V.; Casado, J.; López Navarrete, J. T.; Raimundo, J.-M.; Blanchard, P.; Roncali, J. *Chem.—Eur. J.* **2003**, *9*, 3670. (g) Casado, J.; Hernández, V.; Kim, O.-K.; Lehn, J.-M.; López Navarrete, J. T.; Delgado Ledesma, S.; Ponce Ortiz, R.; Ruiz Delgado, M. C.; Vida, Y.; Pérez-Inestrosa, E. *Chem.—Eur. J.* **2004**, *10*, 3805. (h) Casado, J.; Pappenfus, T. M.; Miller, L. L.; Mann, K. R.; Ortí, E.; Viruela, P. M.; Pou-Amerigo, P.; Hernández, V.; López Navarrete, J. T. *J. Am. Chem. Soc.* **2003**, *125*, 2534. (i) Zerbi, G.; Castiglioni, C.; Del Zoppo, M. *Electronic Materials: The Oligomer Approach*; Wiley-VCH: Weinheim, Germany, 1998; p 345. (j) Casado, J.; Ponce Ortiz, R.; Ruiz Delgado, M. C.; Azumi, R.; Oakley, R. T.; Hernández, V.; López Navarrete, J. T. *J. Phys. Chem. B* **2005**, *109*, 10115.
- (8) (a) Stephens, P. J.; Devlin, F. J.; Chabalowski, F. C. F.; Frisch, M. J. *J. Phys. Chem.* **1994**, *98*, 11623. (b) Novoa, J. J.; Sosa, C. *J. Phys. Chem.* **1995**, *99*, 15837. (c) Casida, E.; Jamorski, C.; Casida, K. C.; Salahub, D. R. *J. Chem. Phys.* **1998**, *108*, 4439. (d) Stratman, R. E.; Scuseria, G. E.; Frisch, M. J. *J. Chem. Phys.* **1998**, *109*, 8218. (e) Tschumper, G. S.; Schaefer, H. F. *J. Chem. Phys.* **1997**, *107*, 2529.
- (9) Scott, A. P.; Radom, L. *J. Phys. Chem.* **1996**, *100*, 16502.
- (10) Gaussian 03, Revision C.02. Frisch, M. J.; Trucks, G. W.; Schlegel, H. B.; Scuseria, G. E.; Robb, M. A.; Cheeseman, J. R.; Montgomery, J. A., Jr.; Vreven, T.; Kudin, K. N.; Burant, J. C.; Millam, J. M.; Iyengar, S. S.; Tomasi, J.; Barone, V.; Mennucci, B.; Cossi, M.; Scalmani, G.; Rega, N.; Petersson, G. A.; Nakatsuji, H.; Hada, M.; Ehara, M.; Toyota, K.; Fukuda, R.; Hasegawa, J.; Ishida, M.; Nakajima, T.; Honda, Y.; Kitao, O.; Nakai, H.; Klene, M.; Li, X.; Knox, J. E.; Hratchian, H. P.; Cross, J. B.; Bakken, V.; Adamo, C.; Jaramillo, J.; Gomperts, R.; Stratmann, R. E.; Yazyev, O.; Austin, A. J.; Cammi, R.; Pomelli, C.; Ochterski, J. W.; Ayala, P. Y.; Morokuma, K.; Voth, G. A.; Salvador, P.; Dannenberg, J. J.; Zakrzewski, V. G.; Dapprich, S.; Daniels, A. D.; Strain, M. C.; Farkas, O.; Malick, D. K.; Rabuck, A. D.; Raghavachari, K.; Foresman, J. B.; Ortiz, J. V.; Cui, Q.; Baboul, A. G.; Clifford, S.; Cioslowski, J.; Stefanov, B. B.; Liu, G.; Liashenko, A.; Piskorz, P.; Komaromi, I.; Martin, R. L.; Fox, D. J.; Keith, T.; Al-Laham, M. A.; Peng, C. Y.; Nanayakkara, A.; Challacombe, M.; Gill, P. M. W.; Johnson, B.; Chen, W.; Wong, M. W.; Gonzalez, C.; Pople, J. A. *Gaussian, Inc.*: Wallingford CT, 2004.
- (11) Becke, A. D. *J. Chem. Phys.* **1993**, *98*, 5648.
- (12) Sosa, C.; Andzelm, J.; Elkin, B. C.; Wimmer, E.; Dobbs, K. D.; Dixon, D. A. *J. Phys. Chem.* **1992**, *96*, 6630.
- (13) (a) Runge, E.; Gross, E. K. U. *Phys. Rev. Lett.* **1984**, *52*, 997. (b) Gross, E. K. U.; Kohn, W. *Adv. Quantum Chem.* **1990**, *21*, 255. (c) Heinze, H.; Goerling, A.; Roesch, N. *J. Chem. Phys.* **2000**, *113*, 2088.
- (14) The bond length alternation pattern (BLA) is calculated as the average value of the difference between the CC distances of connected successive bonds of a given path.

(15) (a) Cornil, J.; dos Santos, D. A.; Beljonne, D.; Bredas, J. L. *J. Phys. Chem.* **1995**, 99, 5604. (b) Beljonne, D.; Cornil, J.; Bredas, J. L.; Friend, R. H. *Synth. Met.* **1996**, 76, 61. (c) Cornil, J.; Beljonne, D.; Heller, C. M.; Campbell, I. H.; Laurich, B. K.; Smith, D. L.; Bradley, D. D. C.; Müllen, K.; Brédas, J. L. *Chem. Phys. Lett.* **1997**, 278, 139. (d) Zojer, E.; Shuai, Z.; Leising, G.; Brédas, J. L. *J. Chem. Phys.* **1999**, 111, 1668. (e) Gierschner, J.; Mack, H. G.; Lüer, L.; Oelkrug, D. *J. Chem. Phys.* **2002**, 116, 8596. (f) Köhler, A.; Beljonne, D. *Adv. Funct. Mater.* **2004**, 14, 11.

(16) (a) Birnbaum, D.; Fichou, D.; Kohler, B. E. *J. Chem. Phys.* **1992**, 96, 165. (b) Oelkrug, D.; Egelhaaf, H.-J.; Gierschner, J.; Tompert, A. *Synth.*

Met. **1996**, 76, 249. (c) Garnier, F.; Horowitz, G.; Valat, P.; Kouki, F. *Appl. Phys. Lett.* **1998**, 72, 2087. (d) Muccini, M.; Lunedei, E.; Taliani, C.; Beljonne, D.; Cornil, J.; Bredas, J. L. *J. Chem. Phys.* **1998**, 109, 10513. (e) Wasserberg, D.; Marsal, P.; Meskers, S. C. J.; Janssen, R. A. J.; Beljonne, D. *J. Phys. Chem. B* **2005**, 109, 4410.

(17) Koopman, T. *Physica* **1933**, 1, 104.

(18) Long, D. A. *The Raman effect. An unified treatment of the theory of Raman Scattering by molecules*; John Wiley & Sons: Chichester, U.K., 2002. Albrecht, C. A. *J. Chem. Phys.* **1961**, 34, 1476.